Int. J. Heat Mass Transfer. Vol. 27, No. 9, pp. 1623–1629, 1984
Printed in Great Britain

0017 9310/84 $3.00 + 0.00
Pergamon Press Ltd.

Critical heat flux in flowing liquid films

R. P. BAINES, M. A. EL MASRI and W. M. ROHSENOW
Department of Mechanical Engineering, Massachusetts Institute of Technology, Cambridge, MA 02139, U.S.A.

(*Received* 12 *October* 1983)

Abstract—Experimental results for the critical heat flux (CHF) and boiling curve in liquid films were found in substantial agreement with recently-reported findings of other investigators. The main liquid film was observed to separate from the heater surface below CHF, leaving a thinner flowing subfilm. Drop deposition from the main film replenished the latter. When this replenishment was insufficient to compensate for subfilm evaporation, CHF occurred. A model based on the trajectories of deposited drops is proposed to explain the form of the correlating equation to within a constant.

1. INTRODUCTION

THIN boiling liquid films are used in a variety of applications. Examples are process evaporators, cooling laser mirrors, and one system proposed for internally cooling gas turbine blades. Reliable prediction of critical heat flux (CHF) is essential in those situations. Monde and Katto [1] measured the CHF for circular discs, 11 and 21 mm in diameter, with a jet of saturated liquid directed at the center. Tests were taken with water and Freon 113, with jet velocities between 5 and 26 m s^{-1}, and diameters of 2 mm. Tests were on upward and downward facing test sections. The data was correlated by equation (1). The nondimensional groups in this equation were obtained by dimensional analysis

$$\frac{q_{CHF}}{\rho_g i_{fg}} = 0.0745 U_f \left(\frac{\rho_f}{\rho_g}\right)^{0.725} \left(\frac{\sigma}{\rho_f U_f^2 D}\right)^{1/3} \quad (1)$$

where D is the diameter of the disc test section.

The nucleate boiling heat transfer curve was approximated by an extension of the pool nucleate boiling curve.

Katto and Ishii [2] measured the CHF on a rectangular copper block, with saturated liquid directed from one side as a jet. Water, Freon 113 and trichloroethane were tested on blocks 15 mm wide and 10, 15, and 20 mm long. The angle of incidence of the jet was varied between 15° and 60° and the thickness of the jet orifice was between 0.56 and 0.77 mm. Data was taken for liquid velocities between 1.5 and 15 m s^{-1} and was correlated by equation (2)

$$\frac{q_{CHF}}{\rho_g i_{fg}} = 0.0164 U_f \left(\frac{\rho_f}{\rho_g}\right)^{0.867} \left(\frac{\sigma}{\rho_f U_f^2 L}\right)^{1/3}. \quad (2)$$

The nucleate boiling data, plotted on a graph of heat flux vs temperature was predicted reasonably well by the pool boiling relation.

Katto and Shimizu [3] measured CHF on a disc 10 mm in diameter with saturated liquid jets directed at its center at velocities up to 20 m s^{-1}. Freon 12 was tested at five pressures between 6 and 27.9 bar and data for water and Freon 113 were taken at atmospheric pressure. The heater was facing downwards. It was found that at a certain velocity the heat flux at CHF stopped increasing with velocity. Data was split into the variable, V, regime and the invariable, I, regime, by equation (4). The boundary between the two regimes is given by the intersection of the two equations resulting in equation (5). The possibility that another regime exists at elevated pressure was suggested by the Freon 12 data taken at 27.9 bar

$$\frac{q_{CHF}}{\rho_g i_{fg}} = 0.188 U_f \left(\frac{\rho_f}{\rho_g}\right)^{0.614} \left(\frac{\sigma}{\rho_f U_f^2 D}\right)^{1/3} \quad (3)$$

$$\frac{q_{CHF}}{\rho_g i_{fg}} = 1.18 U_f \left(\frac{\rho_f}{\rho_g}\right)^{0.614} \left(\frac{\sigma}{\rho_f U_f^2 D}\right)^{1/2} \quad (4)$$

$$\frac{\sigma}{\rho_f U_f^2 D} = 1.64 \times 10^{-5}. \quad (5)$$

Ueda *et al.* [4] studied CHF for a film of saturated liquid falling over a cylinder with its axis mounted vertically, in line with the flow. The cylinder was 180 mm long and 8 mm in diameter. Water, Freon 113, and Freon 11 were used at Reynolds numbers between approximately 1000 and 15 000 corresponding to a maximum film mean velocity of 1.4 m s^{-1}. The nucleate boiling heat transfer curve, CHF, and the rate at which liquid was thrown from the film in fine droplets were studied.

The nucleate boiling heat transfer curve was found to be similar to that for pool boiling. Three regions of CHF were identified. The first two are related to disruption of the film by nucleation and apply at flow rates below the present range of interest. In the third region which applied to the upper range of Reynolds numbers studied, data was correlated by equation (2), even though the length of the heater was 180 mm. Equation (2) was obtained for a range of heaters, the maximum length being 20 mm.

Lienhard and Eichhorn [5] measured the CHF for a vertical upflow of saturated liquid over a fully immersed horizontal cylinder. Above a velocity (of about 0.2 m s^{-1}) given by equation (6), the flow over the cylinder took up a two-dimensional form and CHF was

NOMENCLATURE

a	acceleration
c	constant
C_p	specific heat of liquid
C_{sf}	coefficient in equation (8)
D	diameter
d	drop diameter
g	acceleration of gravity
h	heat transfer coefficient
i_{fg}	latent heat
k	conductivity of liquid
L	length of heater
Pr	Prandtl number of liquid
q	heat flux
R	radius
Re	film Reynolds number
s	exponent of equation (8)
T	temperature
t	time
U_f	film average velocity
u_0	drop initial velocity in x-direction
V_v	vapor superficial velocity normal to heater
v_0	drop initial velocity in y-direction
x, y	coordinates along and normal to heater
x^*, y^*	origin of drop of critical trajectory.

Greek symbols

Δ	denotes difference
μ	liquid viscosity
ν	liquid kinematic viscosity
ρ	density
σ	surface tension
ψ	angle of film separation.

Subscripts

f	liquid
g	vapor
sat	saturated.

Note: unsubscripted properties refer to liquid.

correlated for water, Freon 113, methanol and isopropanol by an equation that can be written as equation (7). This equation shows a close resemblance to equations (1)–(3)

$$\left(\frac{2R\rho_g U_f^2}{\sigma}\right)_{tran} = 4\frac{\rho_f}{\rho_g} R\left[\frac{g(\rho_f-\rho_g)}{\sigma}\right]^{1/2} \quad (6)$$

$$\frac{q_{CHF}}{\rho_g i_{fg}} = 0.0165 U_f\left(\frac{\rho_f}{\rho_g}\right)^{0.833} \times\left(\frac{\sigma}{\rho_f U_f^2 D}\right)^{1/3} + \frac{U_f}{169\pi}\left(\frac{\rho_f}{\rho_g}\right)^{3/4} \quad (7)$$

where D is the diameter of the cylinder and R is the radius.

Below the velocity given by equation (6), CHF was given by the pool boiling correlation for cylinders. Data from a number of papers was used over a range of cylinder radii but velocities over 1 m s^{-1} were tested only for water up to a maximum of 3 m s^{-1}. A mechanism was postulated and used to derive equation (7). It was based on a mechanical energy balance on the vapor envelope and the criterion that when the kinetic energy of the vapor can no longer be absorbed as surface energy, the observed shape of the vapor envelope becomes unstable and CHF occurs. However, it does not seem possible to apply exactly this mechanism to the geometries involving discs and jets which are covered by the same form of equation.

Lienhard and Eichhorn [6] have suggested a mechanism for CHF on discs and improved on the correlation of equation (1) by including the ratio of the disc diameter to the jet diameter and by varying the exponent on the Weber number from $-3/8$ to $-1/3$ to $-1/4$. The mechanism is based on the kinetic energy of the vapor being equal to the surface energy of fine drops created by the boiling just prior to the CHF. At CHF, the liquid layer can no longer absorb all the kinetic energy of the vapor by forming droplets and so it is blown off the heater as coarse drops. Hence, this mechanism predicts that the main film separates as CHF is reached, slightly at variance with the observed behavior, where the main film is seen to be separated at heat fluxes less than the CHF.

In this paper, data taken with water and Freon 113 for plane films is reported. It agrees with the correlations previously published. A mechanistic model based on the dynamics of drops formed by the shattered liquid layer is proposed. This model enables one to derive a basis for CHF correlation to within a numerical constant.

2. TEST APPARATUS AND PROCEDURE

A schematic diagram of the apparatus is shown in Fig. 1. It consists of a long plane channel made of G-10 plastic 75 mm wide. A test section 66 mm wide and 114 mm long was fitted into the channel wall 1.45 m from the top. The channel could be set at different angles from the horizontal.

Experiments were performed with free-falling gravity-driven liquid films as well as with liquid jets issuing from a plane rectangular nozzle. In the latter case, the nozzle was positioned on the channel wall just upstream of the test section, and liquid was supplied to a closed box which fed the nozzle under pressure.

The liquid was pumped through a heat exchanger provided with heating steam coils to bring it to saturation. It then flowed through a rotameter, into the upper tank at the top of the plane channel, or into the nozzle box.

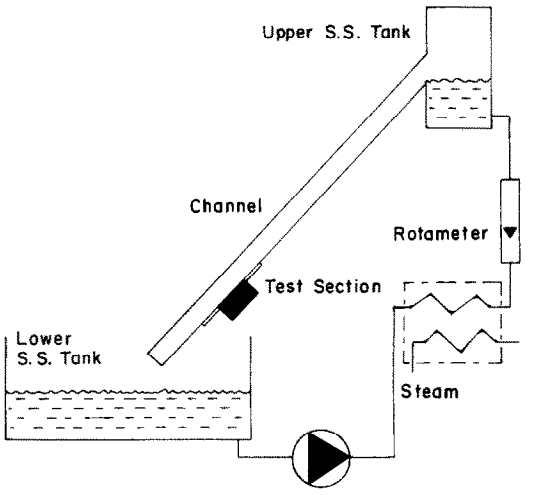

FIG. 1. Schematic of test apparatus.

For the gravity-driven tests, the liquid flowed from the upper tank over a sharp-edged weir into the channel. The long distance along the channel (1.45 m) until the test section assured fully-developed flow. Unfortunately, it also made it difficult to maintain saturation temperature with the Freon tests even when the channel was covered and well insulated.

The test section was a block of oxygen-free copper fitted with ten electric heaters. Pairs of thermocouples were set in holes drilled from the side in two planes parallel to the top surface of the block. Those planes were positioned 5.1 and 15.9 mm from the top surface. The surface temperature was estimated by extrapolating the linear temperature gradient obtained from those thermocouples. Their accuracy was verified by a surface thermocouple. Surface temperature errors due to the uncertainty of the thermocouple junction location within the holes were estimated to be around $\pm 1.5°C$. The heat flux was obtained from the temperature gradient and verified using the electric input to the heaters. Both measurements were within 5% of each other. Three pairs of thermocouples were used in the data. Those were positioned at distances of 19, 45, and 95 mm from the leading edge of the heater.

Prior to each run, the heater surface was cleaned with wire wool and acetone and dried. The liquid was circulated and brought to saturation temperature. The system was run until steady state was established. Typically this took about 1 h.

The power to the heaters was increased in small increments. When a steady reading of the thermocouples occurred, it was recorded and the next increment of power added. At CHF, the test section temperature rose rapidly and a protection device cut power supply. The exact value of CHF occurs somewhere between the flux value when the power tripped and the preceding steady-state condition. Those values are joined by bars in the data plots.

The range of experimental data acquired is given in the Appendix.

3. EXPERIMENTAL RESULTS

Typical plots of heat flux vs surface temperature for water films are presented in Fig. 2. The runs labelled 3 and 43 bound the data taken for water films at 1 atm for both cases of gravity- and jet-driven films. The range of parameters for the data is listed in the Appendix. The solid curve labelled 1 is the Rohsenow pool-boiling correlation

$$\frac{C_p \Delta T_{sat}}{i_{fg}} = C_{sf}\left\{\frac{q}{\mu C_p}\left[\frac{\sigma}{g(\rho_f - \rho_g)}\right]^{1/2}\right\} Pr^s \qquad (8)$$

where C_{sf} and s are taken as 0.013 and 1 [7]. This is in agreement with the findings of previous researchers that the boiling curve for a thin flowing film is reasonably approximated by that for a pool, despite the considerable physical difference between the two situations.

Attempts to correlate the data using flow boiling correlations showed discrepancies. As an example, curve 2 on Fig. 2 is the predicted flow boiling curve for the conditions of run No. 6 calculated using the method of ref. [8]. The heat transfer coefficient for the forced convection contribution used in that calculation was obtained from the recommendation of ref. [9], i.e.

$$h\left(\frac{v^2}{gk^3}\right)^{1/3} = 3.8 \times 10^{-3} Re^{0.4} Pr^{0.65}. \qquad (9)$$

This equation also agrees reasonably with the earlier work by Dukler [10]. Critical heat flux results for the gravity-driven liquid films were taken for Reynolds numbers ranging from 7800 to 74 600 with the channel at 45° and 80° from the horizontal. Critical heat flux was found to occur within a narrow range of fluxes, fairly close to that for a pool, despite the wide range of flow rates. To compare this with the jet-film data, it is plotted on CHF vs average film velocity in Fig. 3. The film velocity was calculated, based on the analysis of Dukler

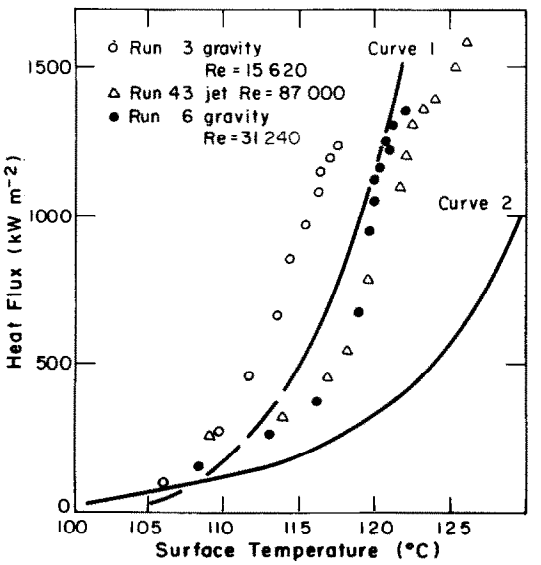

FIG. 2. Nucleate boiling curves for water films.

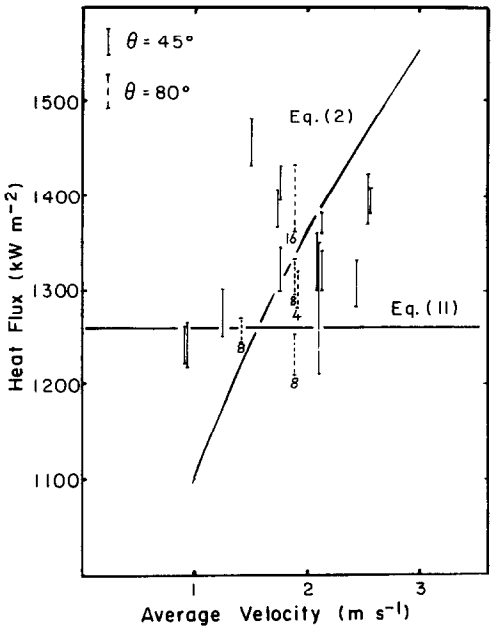

FIG. 3. Critical heat flux for gravity-driven water films.

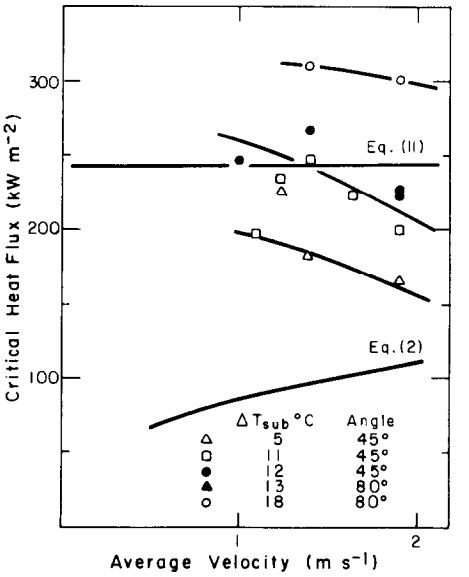

FIG. 5. Critical heat flux for gravity-driven Freon-113 films.

[10], from

$$U_f = 1.25Re^{0.452}(vg \sin\theta)^{1/3}. \quad (10)$$

Also shown on Fig. 3 is the pool boiling CHF given by

$$\frac{q_{CHF}}{\rho_g i_{fg}} = 0.15\left[\frac{\sigma g(\rho_f - \rho_g)}{\rho_g^2}\right]^{1/4}. \quad (11)$$

Critical heat flux results for the jet-driven water film are shown in Fig. 4 plotted vs average velocity. This velocity is obtained by dividing the volume flow rate by the area of the plane nozzle, whose height was 1.33 mm in all cases. This thickness is close to that calculated for the gravity-driven film over much of its data range. The data for the jet film was found independent of whether the plane was horizontal or vertical. Equation (2) correlates this data for velocities up to 2.5 m s^{-1}. At higher velocities, CHF appears to level off at some maximum value as suggested in ref. [4]. Equation (4) of ref. [4] would predict a maximum CHF of 1.72 MW m^{-2} at a U_f of about 4 m s^{-1} for our experimental conditions. This is in reasonable agreement with the data.

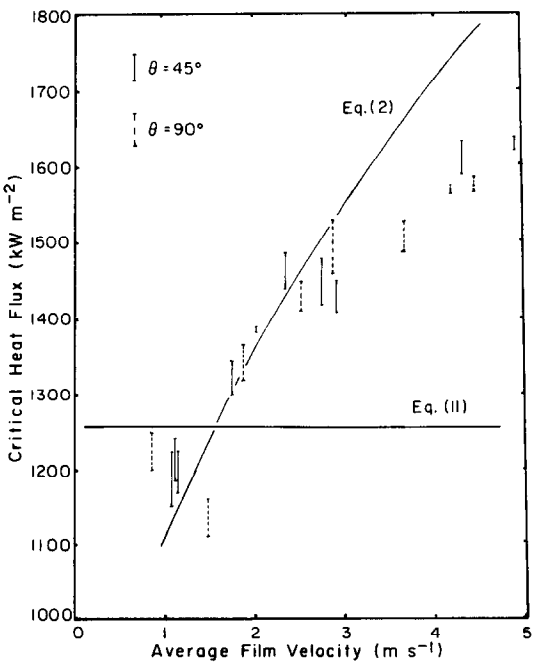

FIG. 4. Critical heat flux for jet-driven water films.

Results for gravity-driven Freon 113 films were obtained for Reynolds numbers in the range 9600–38 400. It was impossible to achieve saturated inlet with the present apparatus so the data was for subcooled flows. Figure 5 shows plots of CHF vs film velocity as calculated from equation (10). The inlet subcoolings are indicated. The data lies below the pool CHF, equation (11) but well above equation (2), indicating that equation (2) is the more appropriate, its underprediction being due to the subcooling. The data approached equation (2) as the subcooling is progressively decreased.

4. EXPERIMENTAL OBSERVATIONS

The mechanism of CHF observed was rather similar to that described by Monde and Katto [1], Kaito and Ishii [2], and Katto and Shimizu [3]. It is illustrated by the series of photographs of plate 1. The photographs are for a jet-driven film on a vertical wall. Average velocity was 1.82 m s^{-1} and Reynolds number about 33 000. The CHF for this run was 1350 kW m^{-2}. Plate 1a (q = 949 kW m^{-2}) shows a side view of the film in stable but vigorous nucleate boiling. As the heat flux was increased, the main film began to separate, leaving

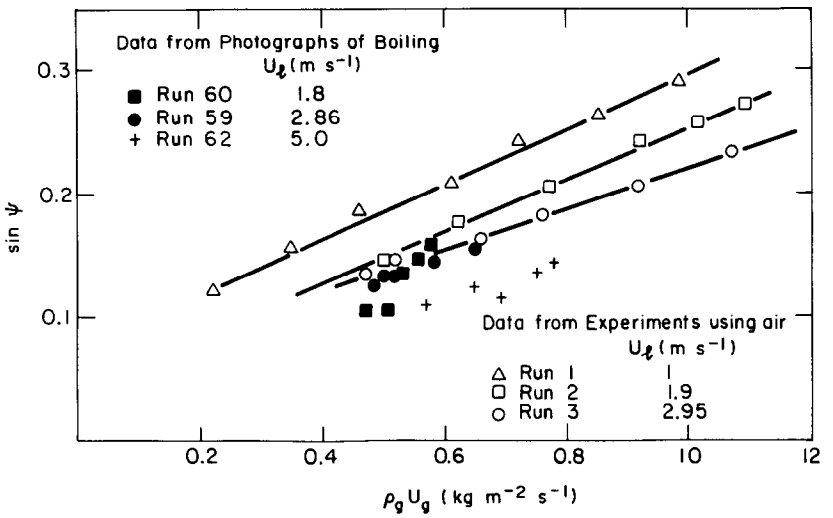

FIG. 6. Relation between film separation angle and mass flux ratio.

a thinner subfilm on the heater surface. The latter continued in nucleate boiling, as seen in plate 1b (q = 1150 kW m^{-2}). With further increases in heat flux, the separated main film shattered into globules and drops. Some deposition of drops back onto the subfilm occurred, but much of the liquid reformed into a turbulent film after passing over the entire length of the heater. Plate 1c (q = 1321 kW m^{-2}) shows conditions just prior to CHF. The thinner subfilm was observed to start forming a dry patch towards the trailing edge of the heater, this dry patch moved upstream as CHF occurred.

To examine to what extent, if any, the subfilm was replenished by drop deposition from the shattered main film a thin sheet metal plate was inserted underneath the separated main film from the downstream end. This prevented any replenishment from the main film. Critical heat flux was observed at lower power levels when this was done. The exact value depended on the width of the metal plate and how far upstream it intruded between the two films. Typically CHF was about 30% lower when this plate was shielding about half the lower film.

The sheet metal plate was also used to deflect the separated main film back towards the wall, causing an increase in CHF.

The angle of the separated main film was observed to decrease at higher liquid velocities. Since the range of vapor velocities, which corresponds to CHFs was rather narrow, it was decided to further investigate this phenomena using a boiling simulation. A similar channel was constructed with a porous plate instead of a heater. Air was blown from the porous plate and the mean separation angle of the liquid film measured. The results are shown in Fig. 6 which indicate an approximate proportionality of the separation angle to the ratio of transverse to film mass fluxes. Figure 6 includes data from the air simulation as well as actual boiling as indicated.

5. MODEL

A mechanistic model based upon the experimental observations is proposed to explain the form of the correlation. Just prior to CHF the main film is separated at a small angle ψ from the leading edge of the heater. In accordance with the observation of Fig. 6, this is proportional to the mass flux ratio

$$\psi = c_1\left(\frac{\rho_g U_g}{\rho_f U_f}\right). \tag{12}$$

The separated film ejects drops as it shatters. The velocity of an ejected drop relative to the film is determined by the proportionality between the retaining surface energy and its kinetic energy

$$v = c_2\sqrt{\left(\frac{12\sigma}{\rho_f d}\right)}. \tag{13}$$

Now, as the experiment with the deflector plate suggests, CHF occurs when the replenishment rate of the subfilm from the main film is inadequate to maintain its flow above the wetting rate. The rate of replenishment is proportional to the length of the main film shedding drops that reach the heater surface. To determine this length we solve for the critical drop trajectory shown in Fig. 7. All drops of diameter d, shed at an initial velocity v_0 in the normal direction will reach the heater if they originate at a location $x < x^*$. Those originating at $x > x^*$ will not reach the heater. Since $\psi \ll 1$ the drop's initial absolute velocity components are essentially $u_0 = U_f$ and v_0 as given by equation (13). The drag due to the vapor emanating from the subfilm at a velocity V_v retards the drop in the y-direction at a rate proportional to the vapor dynamic head and drop frontal area and inversely proportional to its mass, thus

$$\frac{d^2y}{dt^2} = c_3\left(\frac{\rho_g V_v^2}{\rho_f d}\right) = a \tag{14}$$

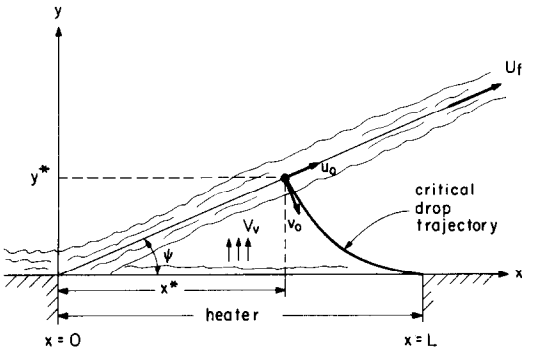

FIG. 7. Model for critical drop trajectory.

neglecting retardation in the x-direction, the drop trajectory is obtained as

$$y = y^* - v_0 t + 1/2at^2 \tag{15}$$

$$x = x^* + u_0 t \tag{16}$$

eliminating t between equations (15) and (16), and noting that the critical trajectory is the one for which $\dot{y} = y = 0$ at $x = L$ and that $y^* = \psi x^*$ gives

$$L = x^* + \frac{u_0 v_0}{a} \tag{17}$$

and

$$\psi x^* = \frac{1}{2}\frac{v_0^2}{a}. \tag{18}$$

Now the replenishment rate is proportional to x^* whereas the depletion rate is proportional to L so that CHF is controlled by their ratio, i.e. occurs when $x^* = c_4 L$. Using this in equations (17) and (18), substituting for ψ and v_0 from equations (12) and (13), respectively, and noting that

$$v_v = \frac{q}{\rho_g i_{fg}} \tag{19}$$

gives CHF

$$\frac{q_{CHF}}{i_{fg}\rho_g} = KU_f\left(\frac{\sigma}{\rho_f U_f^2 L}\right)^{1/3}\left(\frac{\rho_f}{\rho_g}\right)^{2/3} \tag{20}$$

where

$$K = \left(\frac{6c_2}{c_1 c_3 c_4}\right)^{1/3}$$

which is in agreement with the previously given correlations, equations (1)–(3), with a slight difference in the exponents. The constant K, however, cannot be predicted by this approximate argument since the four proportionality constants cannot be determined.

6. CONCLUSIONS

(1) Experimental data on CHF for saturated water films at 1 atm was found to agree with equation (2), previously given in ref. [2].

(2) The CHF for gravity-driven water films displayed larger scatter, thought to originate from the large surface waves.

(3) For jet-driven films, CHF was found to taper off at higher velocities, above 2.5 m s^{-1}, in agreement with previous findings of ref. [4].

(4) Critical heat flux for subcooled gravity-driven Freon films approached equation (2) as the subcooling decreased towards zero.

(5) The nucleate boiling curve for the two types of films was close to that for nucleate pool boiling, despite the difference in physical situations. Flow boiling correlations could not predict it.

(6) A model to explain the form of equation (2), to within a numerical constant, is proposed.

Acknowledgement—The authors are grateful to the National Science Foundation for supporting this research under grant number MEA-8017416.

REFERENCES

1. M. Monde and Y. Katto, Burnout in a high heat flux boiling system with an impinging jet, *Int. J. Heat Mass Transfer* **21**, 295–305 (1978).
2. Y. Katto and K. Ishii, Burnout in a high heat flux boiling system with a forced supply of liquid through a plane jet, *Proc. 6th Int. Heat Transfer Conf.*, Vol. 1, pp. 435–440, Toronto, 7–11 August (1978).
3. Y. Katto and M. Shimizu, Upper limit of CHF in the saturated forced convection boiling on a heated disk with a small impinging jet, *Trans. Am. Soc. Mech. Engrs*, Series C, *J. Heat Transfer* **101**, 265–269 (1979).
4. T. Ueda, M. Inoue and S. Nagatome, Critical heat flux and droplet entrainment rate in boiling of falling liquid films, *Int. J. Heat Mass Transfer* **24**, 1257–1266 (1981).
5. J. H. Lienhard and R. Eichhorn, On predicting boiling burnout for heaters cooled by liquid jets, *Int. J. Heat Mass Transfer* **22**, 1135–1142 (1976).
6. J. H. Lienhard and R. Eichhorn, On predicting boiling burnout for heaters cooled by liquid jets, *Int. J. Heat Mass Transfer* **22**, 774–776 (1979).
7. W. M. Rohsenow, A method of correlating heat transfer data for surface boiling of liquids, *Trans. Am. Soc. Mech. Engrs* **74**, 969 (1952).
8. R. W. Bjorge, G. R. Hall and W. M. Rohsenow, Correlation of forced convection boiling heat transfer data, *Int. J. Heat Mass Transfer* **25**, 753–757 (1982).
9. K. R. Chun and R. A. Seban, Heat transfer to evaporating liquid films, *Trans. Am. Soc. Mech. Engrs*, Series C, *J. Heat Transfer* **91**, 391–396 (1971).
10. A. E. Dukler, Fluid mechanic and heat transfer in vertical falling film systems, *Chem. Engng Prog. Symp. Ser.* **56**(30), 1–10 (1960).

APPENDIX 1

RANGE OF EXPERIMENTAL DATA

	Re	q_{CHF} (kW m^{-2})
Gravity-driven water films	7810–74 600	1232–1397
Jet-driven water films	14 900–90 000	1188–1766
Gravity-driven Freon 113 films	9600–38 400	166–310

FLUX CRITIQUE THERMIQUE DANS LES FILMS LIQUIDES EN MOUVEMENT

Résumé—Des résultats expérimentaux sur le flux critique thermique (CHF) et sur la courbe d'ébullition dans les films liquides sont trouvés en accord convenable avec des résultats de recherches récemment publiés par d'autres expérimentateurs. La partie principale du film se sépare de la surface chauffante au dessous du CHF, laissant une très mince sous-couche en écoulement. Le dépôt de gouttes depuis la partie principale remplit celle-ci. Lorsque ce remplissage est insuffisant pour compenser l'évaporation de la sous-couche, le CHF se produit. On propose un modèle basé sur les trajectoires des gouttes déposées pour expliquer la forme de l'équation qui contient une constante.

KRITISCHE WÄRMESTROMDICHTE IN STRÖMENDEN FLÜSSIGKEITSFILMEN

Zusammenfassung—Experimentelle Ergebnisse zur kritischen Wärmestromdichte (CHF) und zum Verlauf der Siedekurve in Flüssigkeitsfilmen zeigten eine grundsätzliche Übereinstimmung mit kürzlich veröffentlichten Ergebnissen anderer Autoren. Es wurde beobachtet, daß sich der Hauptanteil des Flüssigkeitsfilms vor Erreichen der kritischen Wärmestromdichte von der Heizfläche ablöst und ein dünner strömender Unterfilm zurückbleibt. Ein Tropfenniederschlag vom Hauptfilm erhält den Unterfilm aufrecht. Ist der Tropfenniederschlag nicht mehr ausreichend, um die Verdampfung des Unterfilms zu kompensieren, so wird die kritische Wärmestromdichte erreicht. Es wird ein auf der Flugbahn der niedergeschlagenen Tropfen basierendes Modell vorgeschlagen, das die Form der Korrelationsbeziehung bis auf eine Konstante erklärt.

КРИТИЧЕСКИЙ ТЕПЛОВОЙ ПОТОК В СТЕКАЮЩИХ ПЛЕНКАХ

Аннотация—Измерения авторов критического теплового потока (КТП) и кривой кипения для стекающих пленок хорошо согласуются с данными других исследователей. Показано, что основная часть жидкостной пленки оттесняется от нагреваемой стенки при значениях теплового потока ниже критического, оставляя на поверхности тонкий подслой, пополняемый каплями, осаждающимися из отделившейся части пленки. КТП наблюдается в том случае, когда осаждение капель перестает компенсировать испарение подслоя. Предложена основанная на траекториях осаждающихся капель модель для описания вида обобщенной зависимости с точностью до константы.